

C. J. Litz, Jr.  
Space Systems Laboratory  
McDonnell Douglas Aerospace-West  
Huntington Beach, CA 92647

---

# Laser Doppler Vibrometer: Application of DOE/Taguchi Methodologies to Pyroshock Response Spectra

*Statistical methodologies were employed for measuring and analyzing the explosively induced transient responses of a flat steel plate excited with shock. The application of design of experiment methodology was made to structure and test a Taguchi  $L_9(3^2)$  full factorial experimental matrix (which uses nine tests to study two factors, with each factor examined at three levels) in which a helium-neon laser Doppler vibrometer and two piezocrystal accelerometers were used to monitor explosively induced vibrations ranging from 10 to  $10^5$  Hz on a  $96 \times 48 \times 0.25$  in. flat steel plate. Resulting conclusions were drawn indicating how these techniques aid in understanding the pyroshock phenomenon with respect to the effects and interrelationships of explosive-charge weight and location on the laser Doppler and contact accelerometer recording systems. © 1997 John Wiley & Sons, Inc.*

---

## INTRODUCTION

The helium-neon (HeNe) laser Doppler vibrometer (LDV) was compared in an experimental fully factorial nine-test series with a baseline contact accelerometer (accelerometer A) and a state of the art accelerometer (accelerometer B). Detailed statistical analysis was performed on the data derived from the three recording instruments, which indicated superiority of the LDV in certain areas.

## Pyroshock

Pyrotechnic shock, or pyroshock, is a short-duration, high-amplitude, high-frequency transient structural response that occurs in aerospace-vehicle structures. Transients are generally initi-

ated by the firing of an ordnance item (containing explosive or other energetic propellants as a one-shot item) to separate or release a structural member or fastener. The transient responses usually result from explosive and impact events within the ordnance item as well as from forces associated with the release of strain energy.

The most severe shock source of all spacecraft pyrotechnic devices derives from the explosive severance of the missile skin for stage separation. Typically, this is accomplished through use of linear-explosive mild detonating cord or linear-shaped charge, with the shock environment depending on the thickness of the material cut ( $T$ ) and the amount of explosive charge (grains per foot  $\times$  total length in feet = weight in grains). The separation distance from the explosive and

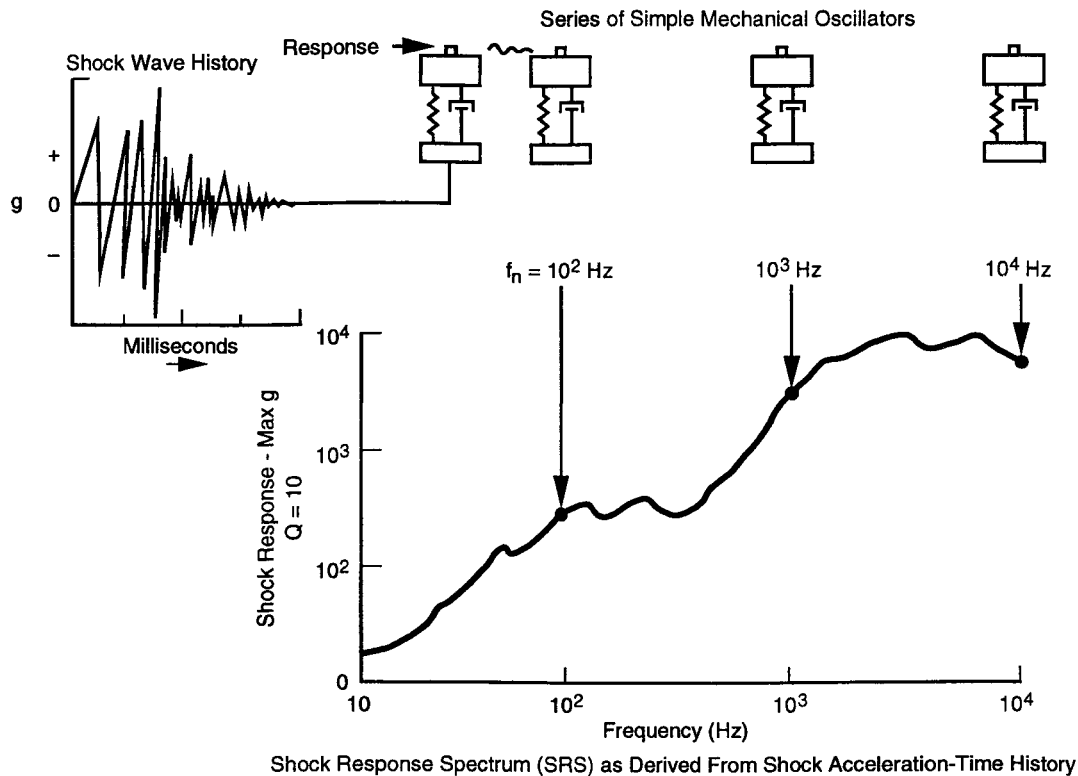


FIGURE 1 Development of shock response spectra.

joints has an effect as well, as shown later in this article. The shock near the explosive source is characterized by a high-amplitude, high-frequency accelerating time history. The shock-response spectrum (SRS) (Fig. 1) is used to describe the frequency content of pyroshock transients in a manner relating to its damage potential, with the SRS representing the maximum acceleration response of each of a series of single degree of freedom system mechanical oscillators that are base driven by the shock-time history. Shock transients that have equivalent response spectra have equivalent damage potential.

#### EVALUATION OF RECORDING INSTRUMENTATION AND TEST-BED PLATE SIZING FOR REPEATED TESTS

In efforts to resolve questions on the use of the laser as a pyroshock recording instrument, a Taguchi  $L_9(3^2)$  full factorial experiment was designed and run. A new test-bed plate was designed and fabricated for repeated tests. The explosive used, Primaline, was placed at three different locations on the plate: back, back offset, and side. A

replaceable 90° steel (ASTM A36) insert on the back of the plate was used to support the Primaline explosive at a 1.5-in. offset. Figure 2 shows the 1T66813 universal steel test-bed plate (96 × 48 × 0.25 in.) that was successfully used for design of experiment (DOE) testing. Also illustrated is the plate in relation to the locations of the LDV and the accelerometers. The two accelerometers were in close proximity and were the same distance from the explosive. The laser beam was focused onto the front of the plate in the same area.

#### LDV

The LDV used in this experiment consisted of an electronics/drive unit with a sensor/optics head joined by a 5-m long interconnection cable. The sensor/optics head contains a small HeNe laser (wavelength 633 nm, red, laser safety class 2). In operation, the laser output is split internally into two beams: an internal reference beam and a probe beam that exits the sensor/optics head through the front focus lens. The standoff distance of the sensor/optics head is continuously adjustable from 0.3 m to infinity. The probe beam forms

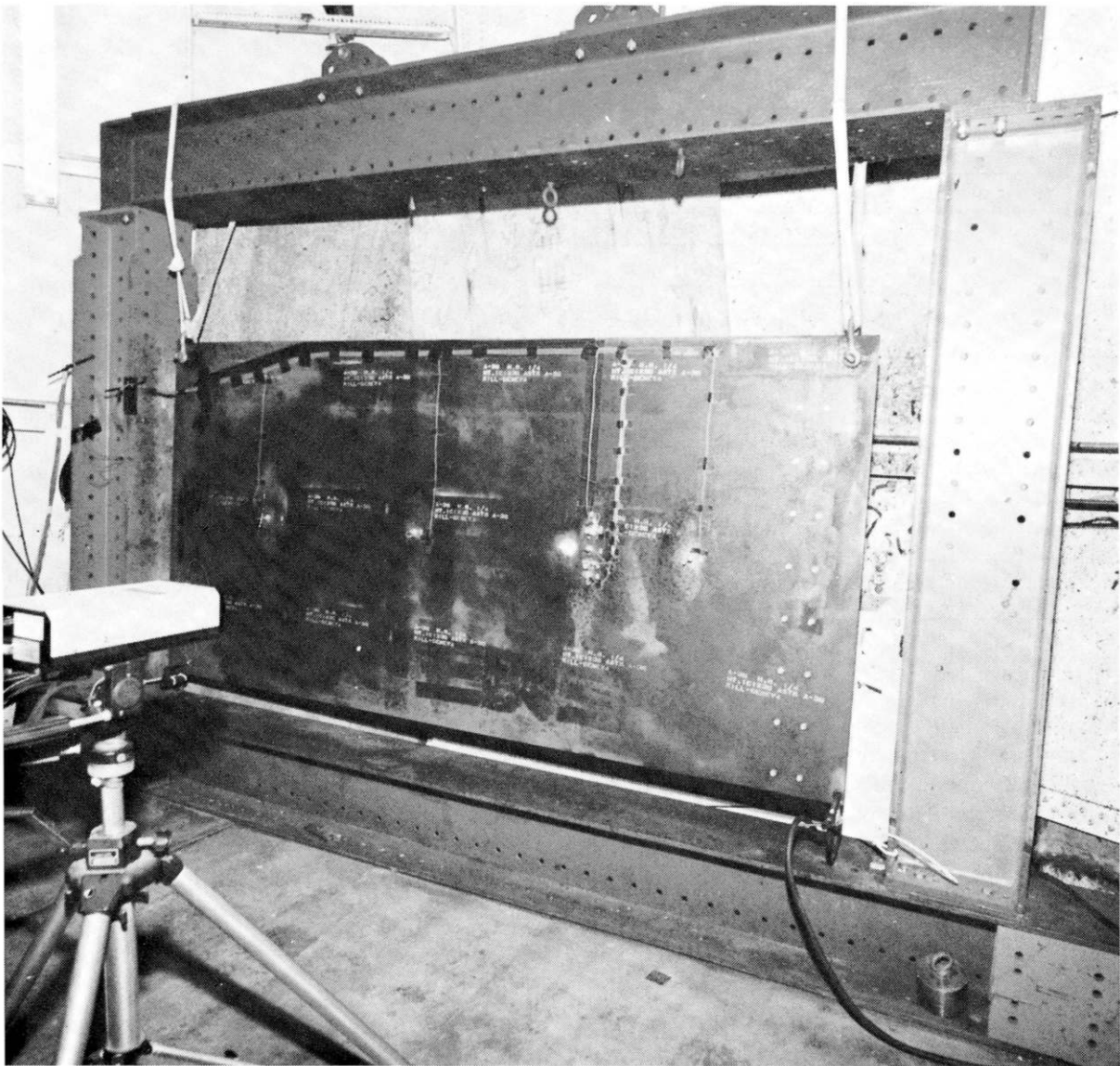


FIGURE 2 Test plate setup, laser vibrometer.

a focus on the target. The same front focus lens collects backscattered light from the target.

The backscattered light experiences a Doppler shift in frequency, the magnitude of which is proportional to the velocity component of the target along the direction of the laser beam. The shift,  $f_d$ , is represented by the following equation:

$$f_d(t) = 2\nu(t)/\lambda, \quad (1)$$

where  $\nu(t)$  is the time-dependent velocity of the target and  $\lambda$  is the wavelength of the laser, 633 nm. The returning probe beam is mixed with the internal reference beam inside the sensor/optics

head at an optical detector. The detector records  $f_d(t)$  and sends this information to the electronics/drive unit. In the electronics/drive unit, a fast linear FM decoder changes the instantaneous Doppler shift frequency  $f_d(t)$  into a calibrated analog voltage proportional to  $\nu(t)$  (Valentekovich et al., 1989). The resulting acceleration–time history is used to generate the SRS using Structure Dynamic Research Company’s software Ideas (see Fig. 1).

## EXPERIMENT DESIGN

The  $L_9(3^2)$  DOE test matrix, which is structured to measure linear and quadratic effects, is illus-

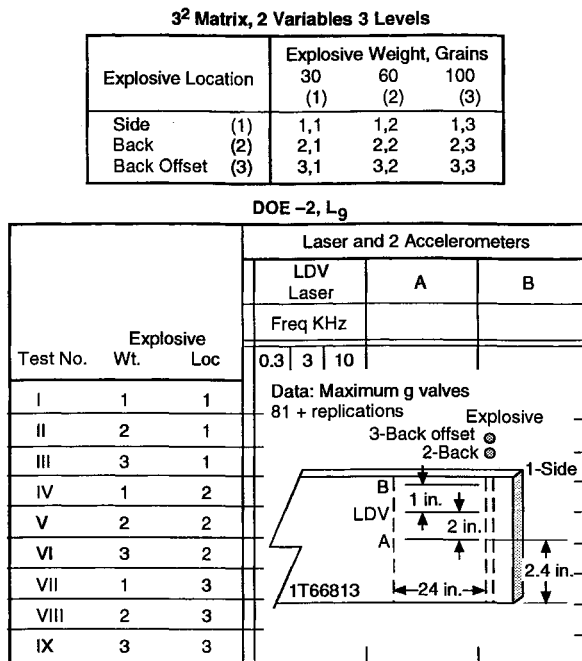


**FIGURE 3** Design of experiment.

trated in Figure 3. As shown, there are a total of nine entries. This matrix addresses two test input variables: frequency and amount of Primaline explosive. The three means used to measure the acceleration output are listed below. The baseline accelerometer (A) was placed 24 in. from the explosive on the center line of the 1T66813 plate. Accelerometer B was placed 3 in. above accelerometer A, and the laser beam was focused in between, 2 in. above the baseline accelerometer. The statistical analysis was performed using the resulting SRS plots for maximum, *g*, at frequencies of 300, 3000, and 10,000 Hz. Additional tests were run to generate more data and hence to improve the estimation of experimental error. There was a total of 102 pieces of data. All main effects and interactions are estimated by a high resolution.

**Contact Accelerometers**

Shock accelerometer A is a self-generating, spring-mass, piezoelectric transducer with a mounted resonant frequency between 40 and 100 kHz. Shock accelerometer B has an integral mechanical filter that provides a 24 dB per octave rolloff above 10 kHz.

**LDV**

The LDV is a noncontact velocity transducer that works on the principle of measuring the Doppler

shift of a laser beam backreflected from a moving target. It uses an HeNe laser with a 633-nm wavelength.

**Primaline Explosive**

Commercial linear explosive with core loads of 7.5, 15, and 25 grains/ft of pentaerythritol tetranitrate was used in 4-ft lengths. The Primaline explosive weights of 30, 60, and 100 grains comprised the total weight. The linear Primaline was placed on the side, back, and back offset of the plate. The electroexplosive device (Instadet No. 6) was taped at the end of the explosive line.

**Analyses**

Regression analysis (Box et al., 1978) was utilized to establish a mathematical model with the ability to predict the maximum acceleration measured by each accelerometer at each of the three locations on the test plate. This model relates the dependent factor (maximum acceleration) to the independent experimental factors (Primaline explosive size and measurement frequency). Primaline location was not treated as a variable for this analysis but was considered in subsequent analyses.

Because the experiment studied each independent factor at three levels, the analysis yielded a quadratic model as follows:

$$y = b_0 + b_1 X_1 + b_2 X_2 + b_{12} X_1 X_2 + b_{11} X_1^2 + b_{22} X_2^2, \tag{2}$$

where *y* is the dependent factor (maximum acceleration), *b*<sub>0</sub> is the intercept parameter, *b*<sub>1</sub> is the slope parameter, and *X*<sub>1</sub> are the independent factors (Primaline explosive charge and frequency).

To supplement the parameter estimates derived from the regression, an analysis of variance (ANOVA) table was also generated. (ANOVA is a statistical technique that assesses the statistical significance of the regression model.) Calculations performed in the ANOVA were based on the fundamental equation that decomposes the total variation in the experimental results into components representing the variability due to the independent experimental factors under study (Primaline explosive charge and frequency) and the variability due to random experimental error when the same factors are kept constant.

$$\sum \sum (y_{ij} - \bar{y})^2 = n \sum (\bar{y}_j - \bar{y})^2 + \sum \sum (y_{ij} - \bar{y}_j)^2, \tag{3}$$

**Table 1. Comparison of Predicted Versus  $g$  Values**

Frequency (Hz)	Maximum Acceleration (g)	
	Actual	Predicted
300	390	891
3000	4200	4821
10,000	18,000	16,887

LDV, explosive on back of plate.

where  $\sum\sum(y_{ij} - \bar{y})^2$  is the total sum of squares,  $n\sum(\bar{y} - \bar{y})^2$  is the sum of squares due to experimental factors, and  $\sum\sum(y_{ij} - \bar{y}_j)^2$  is the sum of squares due to experimental error.

The ANOVA culminates in an  $F$  test that evaluates the ratio of the variance due to the independent experimental factors to the variance due to experimental error as follows:

$$F = \frac{[n\sum(\bar{y}_j - \bar{y})^2]/(k - 1)}{[\sum\sum(y_{ij} - \bar{y}_j)^2]/(N - k)}, \quad (4)$$

where the larger the ratio, the greater the significance of the experimental factors.

Also reported in the output are  $R^2$ , which are the coefficients of determination (coefficient of correlation squared), and root mean square error (RMSE).  $R^2$  can be interpreted as the percentage of variation in the experimental results that can be explained by the regression model, whereas RMSE quantifies the uncertainty of the predicted response in a manner analogous to the standard deviation of the residuals (predicted minus actual response). The high  $R^2$  and a small RMSE indicated that the model did a good job of predicting the outcome with only a small error. Models developed from the regression analysis were used to create 3-dimensional response-surface (RS) plots that visually depicted the relationship between the dependent and independent variables.

Nine separate printouts were generated (i.e., one was generated for each of the three recording instruments at each of the three Primaline explosive locations on the test plate). The analyses indicated that the model as a whole was statistically adequate. As an example of the prediction equation, all of the numerical values listed under the parameter estimate were used in the quadratic model [Eq. (2)] to predict performance for the maximum Primaline charge of 100 grains on the back of the plate. Thus, maximum acceleration,  $g = 7195 - 0.54$  (frequency, Hz)  $- 277$  (Primaline weight, grains)  $+ 0.019$  (frequency, Hz) (Primaline weight, grains)  $+ 0.000027$  (frequency, Hz)<sup>2</sup>  $+ 2.1$  (Primaline weight, grains)<sup>2</sup>. Table 1 shows a com-

parison between the actual and predicted values for maximum acceleration,  $g$ .

Figure 4 is a plot comparing the predicted and actual maximum  $g$  values as a function of frequency. Figure 5 is the SRS log-log plot of actual test no. 18, with the predicted  $g$  values added for comparative purposes. The close agreement between predicted and actual maximum  $g$  is especially evident at the 3000- and 10,000-Hz frequencies. In some instances the predicted values were not in close agreement with the actual data, as illustrated above. Subsequent residual analysis indicated that a closer agreement of the predicted maximum  $g$  values to the actual values could be obtained with more test data at additional Primaline weights. The prediction equation would have a better fit with the independent factor,  $x$ , expressed in a third-degree ( $x^3$ ) rather than a second-degree ( $x^2$ ) polynomial equation.

### Analysis of Response Surface Plots

Nine RS plots were generated and examined to compare in groups of three the performance of the three recording systems one to another with Primaline at the same location on the plate. The two accelerometers and the LDV beam focus were all located on the front of the plate in the same area, as illustrated in Fig. 2. The following is a summary of these visual comparative analyses.

**Back of Plate.** Results derived from the Primaline arrangement on the back of the plate are shown in Figs. 6, 7, and 8.

The LDV RS plot (Fig. 6), which is slightly concave, illustrates a gradual increase in acceleration with increasing explosive-charge weights of 30, 60, and 100 grains. As expected, there is a similar linear increase in  $g$  through the increasing frequency range from 300, 3000, and 10,000 Hz for a given explosive weight. Overall, the entire surface shape takes the form of a slightly concave plane with a constant slope with increases in  $g$  value with increasing explosive charge.

The contact-accelerometer RS plots (Figs. 7, 8) illustrate interesting phenomena in that both indicated an initial  $g$  value at 0 Hz. Contact accelerometer B (Fig. 7) has a convex surface shape similar to the top of an airfoil. The rolloff at 10,000 Hz is evident at the 100-grain explosive charge. Contact accelerometer A (Fig. 8) illustrates a rapid increase in  $g$  value at increasing Primaline weights and frequencies, especially at 10,000 Hz. The possible onset of accelerometer case resonance may

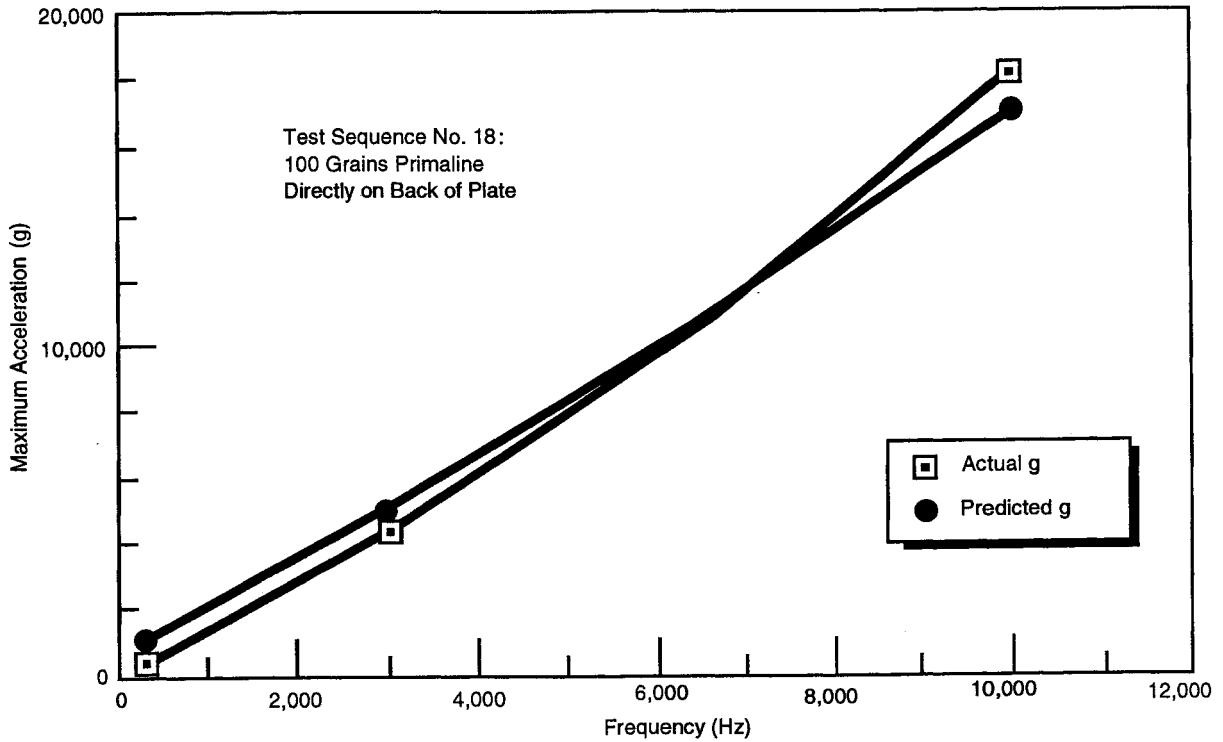


**FIGURE 4** Comparison of predicted vs. actual maximum acceleration, g values (LDV, explosive on back of plate).

be seen at the high g value of 10,000 Hz and a 100-grain explosive charge.

Overall, the three RS plots derived from regression equations for explosive on the back of the plate follow the actual recorded data.

**Back Offset.** Response-surface plots derived from the placement of the Primaline on the back

of the plate at an offset distance had lower g values for all three recording systems with explosive at an offset distance from the plate than with explosive in direct plate contact. This is normal in that the offset and interface attenuate shock transmissibility. However, all three plots had negative g values at low frequencies. As noted earlier, this re-

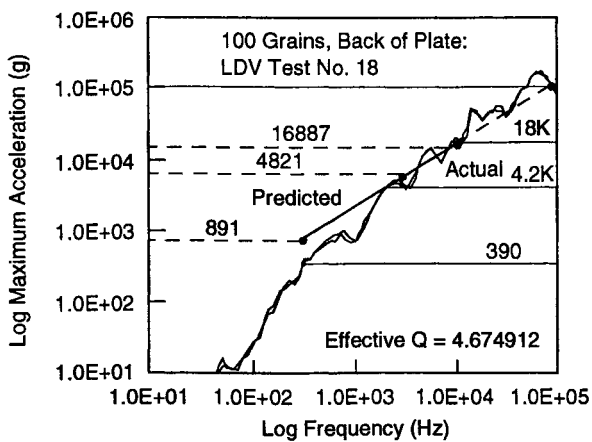


**FIGURE 5** LDV SRS plot, comparison of predicted vs. actual maximum g values.

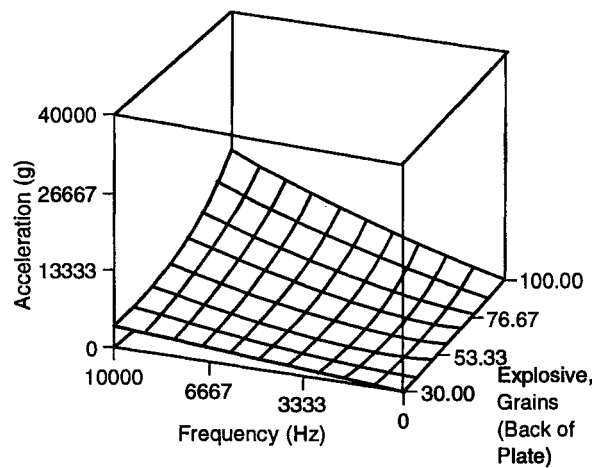


**FIGURE 6** RS plot, laser Doppler (explosive on back of plate).

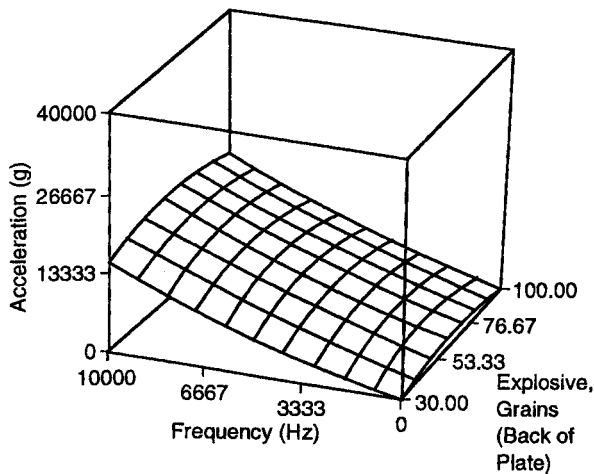


FIGURE 7 RS plot, accelerometer B (explosive on back of plate).

sults from the nature of the regression equations from which the RS plots were generated.

The laser RS plot resembled a flat plane with a general slope increasing in g value and frequency for a given explosive charge. The increase in slope of the g values was more evident at the 100-grain explosive-charge weight. Overall, the surface indicates a stable, gradual variation throughout. Accelerometer B RS plot was slightly convex with increasing g values at larger explosive weights. This surface indicated a less stable condition than that associated with the LDV. Accelerometer A RS plot was slightly concave in the middle, with larger g values than the other two recording systems.

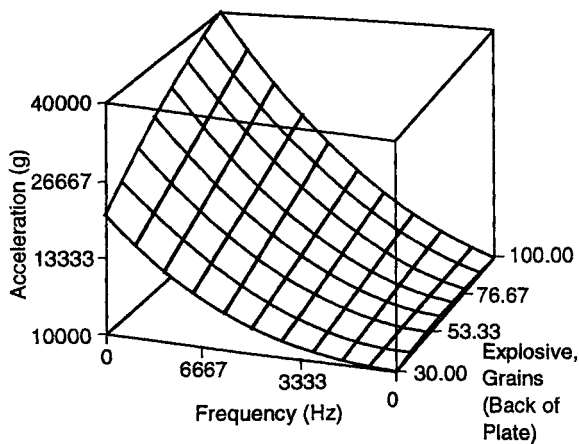


FIGURE 8 RS plot, accelerometer A (explosive on back of plate).

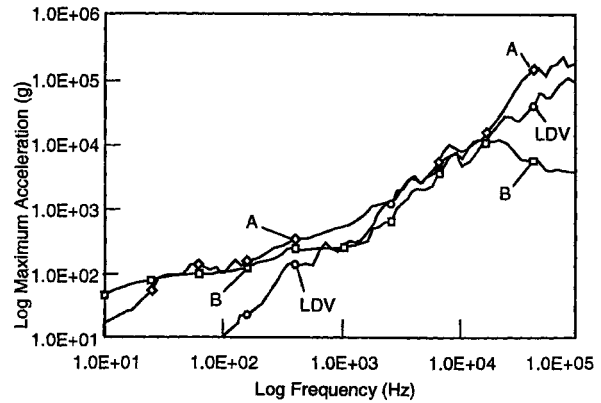


FIGURE 9 SRS comparison of three acceleration histories.

**Side of Plate.** Although located on the side of the plate, the explosive still sends shock waves that drive the plate in the radial as well as transverse directions. Therefore, the level of g values was less than that of the other six RS plots. The three RS plots had lower g values, and the surface plots were not the same slope as those previously illustrated for the explosive on the back of the plate owing to the lower g values on the vertical axis of the RS plots.

The LDV surface RS plot was a flat surface, but the RS plot for accelerometer A was characterized by rapid-magnitude changes in g value, with gradual changes in explosive weight indicating an unstable condition.

Overall this comparative analysis of the nine RS plots indicated the superiority of the LDV recording system as more stable than the two contact accelerometers.

### Comparative Analysis of SRS Acceleration Histories

To allow for comparison of the performance of the three instruments, the SRS acceleration histories of these instruments for the same test were combined into a single plot in Figure 9.

On the basis of the SRS plots in Figure 9, the following was deduced:

1. Both of the contact accelerometers (A and B) show a high acceleration offset at the low-frequency regime of the SRS, whereas the LDV indicates an initial onset at 100 Hz. The LDV acceleration levels are decades lower in the 100–300 Hz regime than those indicated by the two accelerometers—an outcome that

**Table 2. Summary of Taguchi Analysis**

Recording Instrument System	Frequency (Hz)	Signal to Noise Ratio Nominal Is Best (dB)
Contact accelerometer A	300	-1.96
	3000	
	10,000	
B	300	-1.43
	3000	
	10,000	
LDV	300	+0.514
	3000	
	10,000	

can be considered more credible. The LDV is particularly accurate in measuring small displacements associated with the higher frequencies of the dynamic, explosively induced shock waves and their resulting plate motion.

2. Accelerometer B has a rolloff in frequency at 10,000 Hz that appears in this plot. A mechanical filter is incorporated into this accelerometer model to reduce overexcitation caused by a pyroshock environment.
3. Accelerometer A has a case resonance at 37 kHz that contributes to the higher peak acceleration. The accelerometer resonance noise can nullify pyroshock data such that the measured acceleration of a resonating accelerometer is not the environment that the test specimen experiences.

It is also of interest to note that the SRS obtained in a subsequent study (Lieberman et al., 1992), which compared an optical HeNe laser Doppler displacement meter with the same contact accelerometers described herein, generated similar acceleration histories. Specifically, the laser Doppler results obtained in this study were again found to be more representative of actual plate motion than those of the accelerometers, particularly in the low and high frequencies. A general agreement in the midfrequency range with contact accelerometers was also demonstrated.

## TAGUCHI METHODOLOGY

The Taguchi-type orthogonal array is illustrated in Table 2. The signal to noise (S/N) ratio reflecting the amount of variation present for each of the three recording systems was computed for the respective maximum  $g$  values (the  $g$  values are

not shown in the table). The nominal is best (N/B) was then computed. The expression  $S/N_{NB} = 10 \log[(SSm - Ve)/(NVe)]$  is a function of both variability ( $Ve$ ) and average ( $SSm$ ). From this it is evident that reduced variation relating to average causes an increase in the S/N value. The S/N is always a "higher the better" characteristic (not the absolute value in case of negative decibel values) (Ross, 1988).

The N/B analysis yielded

$$S/N_{NB} = 10 \log \left[ \frac{(SSm - Ve)}{NVe} \right], \quad (5)$$

where

$$SSm = T^2/N, T = \sum_{i=1}^N y_i, \quad (6)$$

$$Ve = (SD)^2 = \left[ \frac{\sum_{i=1}^N (y_i - \bar{y})^2}{N-1} \right] = \sum_{i=1}^N \frac{y_i^2 - SSm}{N-1}. \quad (7)$$

The LDV had a higher  $S/N_{NB}$  value (+0.514) than contact accelerometers A or B (Table 2). SD is the standard deviation.

In the experimental design of the experiment the controllable variables (explosive weight and location) were arranged in the orthogonal table (see Fig. 3).

For this analysis there are nine experimental tests: one for each of the nine combinations of the variables. Using Eq. (5) the  $S/N_{NB}$  ratios were calculated for the three different recording instruments for all nine test firings using the numerical  $g$  values for the respective frequencies of 300, 3000, and 10,000 Hz.

The three instruments were at the same relative location on the steel plate equidistant from the explosive so that each received the same relative amount of vibration stimuli for each of the nine firings. The  $S/N_{NB}$  was used to mathematically rate the  $g$ -value variance.

In this analysis the ratio of the power of the signal ( $g$  value) to the power of the noise was computed. The noise includes such factors as material imperfections, manufacturing imperfections, environmental variations, and other factors the instrument manufacturer does not control.

Contact accelerometers A and B have more noise factors than the LDV. These factors are directly impacted by the explosive shocks induced into the plate while the LDV instrument is not violently shock impacted. The only LDV contact



with the plate is the laser light beam. The contact accelerometers can break down during such shock tests while the laser beam, because of its separation from the steel plate, is not affected.

The resulting  $S/N_{NB}$  listed for each instrument in Table 2 is the average for the nine tests. In the Taguchi transformations the  $S/N$  is always interpreted as the larger the  $S/N$  ratio the better (Ross, 1988).

## CONCLUSIONS

On the basis of the LDV analyses presented, the following conclusions can be drawn:

1. The LDV used in the pyroshock experiment is superior to the two contact accelerometers at both the low (100–300 Hz) and high (10,000–30,000 Hz and above) frequencies with respect to its ability to accurately depict the environment.
2. The LDV tracks well in the 600–10,000 Hz frequency range, matching the performance of the two contact accelerometers in that range.
3. The LDV noncontact to the test plate with Primaline is not subjected to intrinsic or mounting resonance. Velocity sensing of the LDV does not strain the limits of the dynamic range as much as with contact-mounted accelerometers.
4. The LDV is not saturated by the strong initial compression waves generated by Primaline in pyroshock tests.
5. The application of DOE and Taguchi methodology to the structure and conduct of pyroshock experiments as well as to the analysis of the resulting data indicates that certain advantages accrue from the use of the LDV

and, further, that specific cost savings can be realized through less testing, use of prediction equations, and understanding of the interrelations of explosive weight, acceleration, and vibration frequency.

6. These techniques offer a totally new dimension toward understanding pyroshock phenomena with respect to the effect and interrelationships of explosive-charge weight and location on the different recording instrumentation systems and the SRSs thus generated.

## RECOMMENDATIONS

It is recommended that more tests and analyses be performed to generate a better fit of prediction equations as well as to validate the above conclusions concerning the credibility of performance comparisons of contact accelerometers with the LDV.

## REFERENCES

- Box, G. P., Hunger, W. G., and Hunter, J. S., 1978, *Regression Analysis—Statistics for Experiments an Introduction to Design, Data Analyses, and Model Building*, Wiley, New York, pp. 453–509.
- Lieberman, P., Czajkowski, J., and Rehard, J., 1992, “Optical System for Measurement of Pyrotechnic Test Accelerations,” *Journal of the IES*, Vol. 35, pp. 25–39.
- Ross, P. J., 1988, “Taguchi Techniques for Quality Engineering,” McGraw-Hill, New York, pp. 167–176.
- Valentekovich, V. M., Navid, M., and Goding, A. C., 1989, “Laser Doppler Vibrometry Measurements of Pyrotechnically Induced Shock,” in *Proceedings of the 60th Shock and Vibration Symposium*, Part 1, pp. 259–271.



Hindawi

Submit your manuscripts at  
<http://www.hindawi.com>

